SUPPLEMENTARY INFORMATION FILE

TITLE

Targeting the disordered C-terminus of PTP1B with an allosteric inhibitor

Navasona Krishnan[1], Dorothy Koveal[2], Daniel H. Miller[3], Bin Xue[1,4], Sai Dipikaa Akshinthala[1], Jaka Kragelj[5], Malene Ringkjøbing Jensen[5], Carla-Maria Gauss[1], Rebecca Page[2], Martin Blackledge[5], Senthil K. Muthuswamy[1,6], Wolfgang Peti[3] and Nicholas K. Tonks[1]*

1. Cold Spring Harbor Laboratory, 1 Bungtown Road, Cold Spring Harbor, New York 11724, USA
2. Department of Molecular Biology, Cell Biology and Biochemistry, Brown University, Providence, RI 02903, USA
3. Department of Molecular Pharmacology, Physiology and Biotechnology, and Department of Chemistry, Brown University, Providence, RI 02903, USA
4. Present address: Department of Molecular & Cell Biology, University of California Berkeley, Berkeley, CA 94720, USA
5. Protein Dynamics and Flexibility, Institut de Biologie Structurale Jean-Pierre Ebel, CEA, CNRS, UJF UMR 5075, 41 Rue Jules Horowitz, Grenoble 38027, France
6. Ontario Cancer Institute, Campbell Family Institute for Breast Cancer Research, Department of Medical Biophysics, University of Toronto, Toronto, Canada

* Correspondence to:

N. K. Tonks: tonks@cshl.edu

SUPPLEMENTARY RESULTS

Supplementary Figure 1. MSI-1436 was a non-competitive inhibitor of PTP1B

a. PTP1B (5 nM) was titrated with the substrate DiFMUP (0-50 μM) in the absence (●) and presence of MSI-1436 at 0.5 μM (■), 1 μM (▲), 2 μM (▼) respectively.

b. Plot of K_m as a function of concentration of MSI-1436 to show that substrate binding affinity remained unchanged in the presence of MSI-1436 (upper panel). Plot of V_{max} against varying concentration of MSI-1436 to show a decrease in the rate of catalysis (lower panel). Values were obtained from nonlinear regression analysis in **A**. Data represent mean ± s.e.m from three independent experiments.

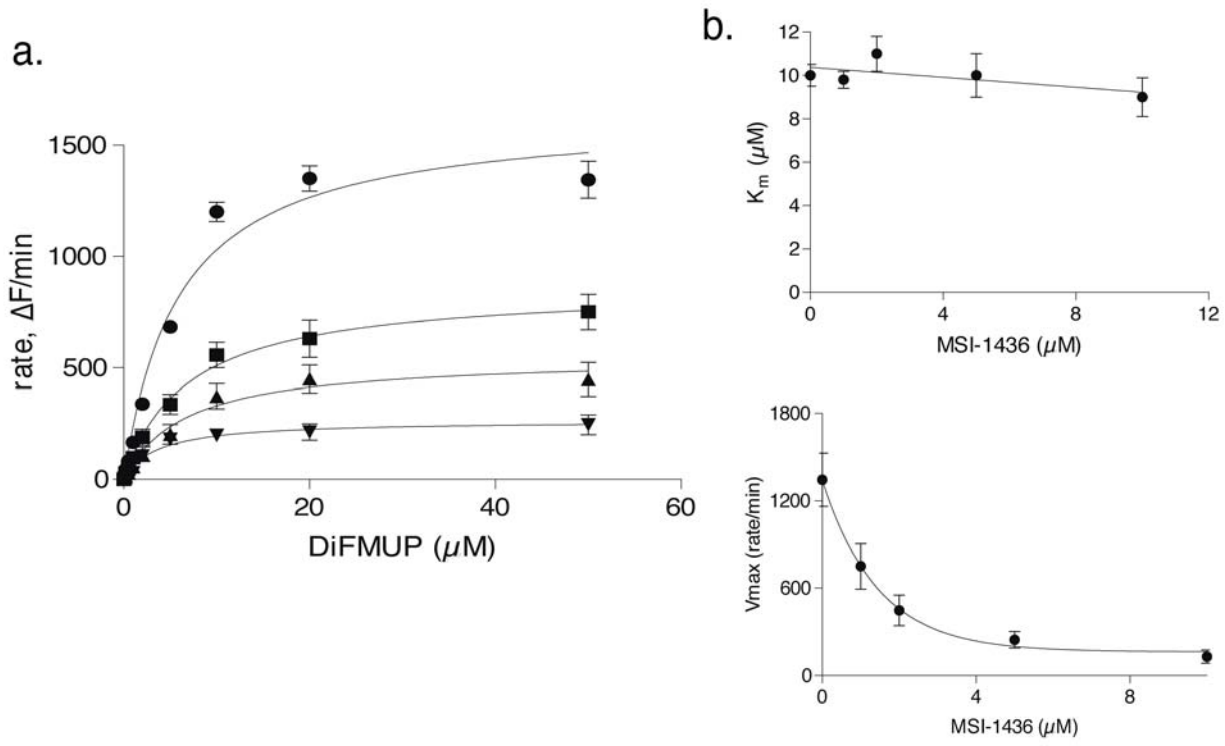

Supplementary Figure 2. Reversibility of inhibition by MSI-1436

$PTP1B_{1-405}$ (50 nM) was incubated without (open circles) and with (closed circles) MSI-1436 (5 μM) for 5 minutes in assay buffer. Following incubation, reversibility was checked by dilution by assaying enzyme (0.5 nM) from the mixture with DiFMUP (10 μM). Data represent mean ± s.e.m from three independent experiments.

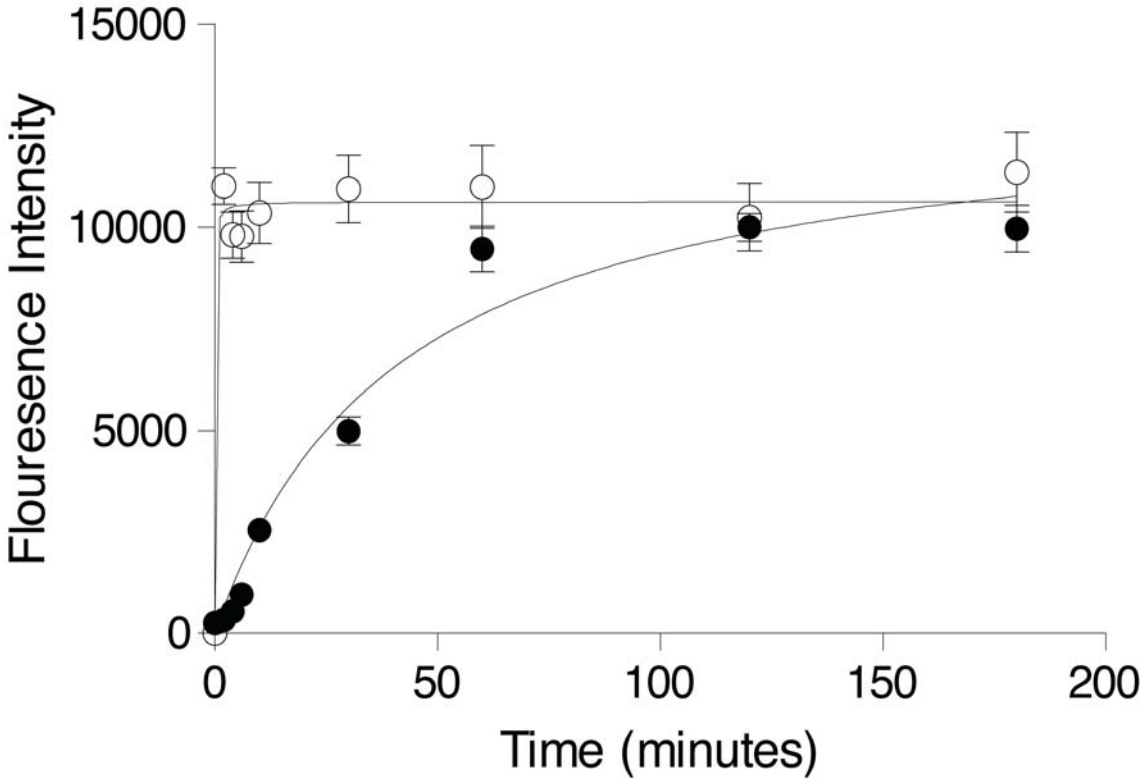

Supplementary Figure 3. Dynamic light scattering mass distribution histogram.

a. PTP1B$_{1\text{-}301}$ and **b** PTP1B$_{1\text{-}393}$. An identical buffer solution was used in both experiments (50 mM HEPES pH 6.8, 150 mM NaCl, 0.5 mM TCEP) and the experiments were performed in triplicate using a Viscotek 802 DLS instrument (Malvern).

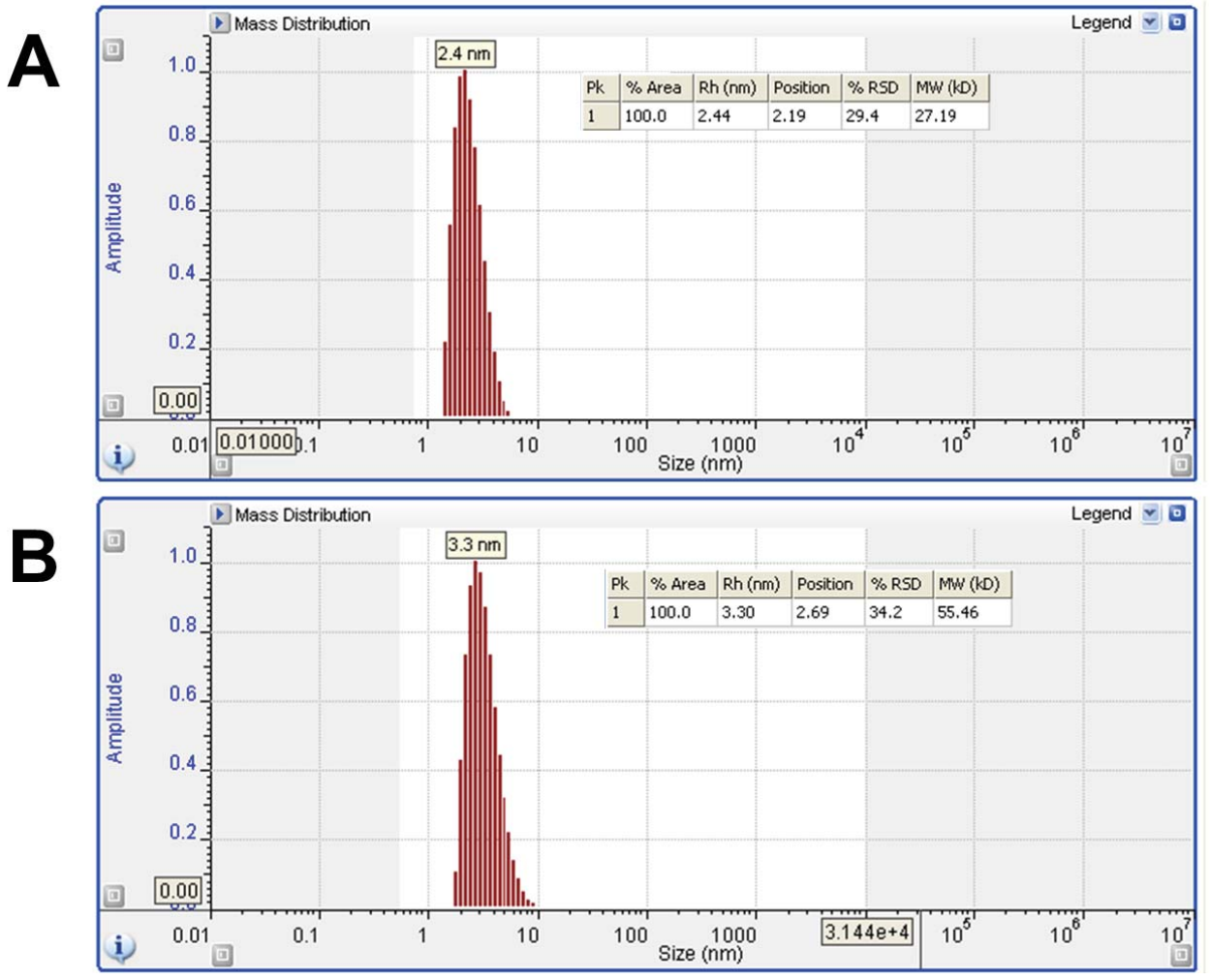

Supplementary Figure 4. **Gel filtration analysis of PTP1B$_{1-405}$ in the absence and presence of MSI-1436**

Elution profile of PTP1B$_{1-405}$ in the absence (black) and presence (blue) of MSI-1436 (upper). In both cases PTP1B$_{1-405}$ eluted as a monomer. The elution volumes were used to calculate the molecular weight of 47k and 43k in the absence and presence of MSI-1436, respectively. The elution of molecular weight standards is indicated by arrows. Fractions eluted from the gel filtration column were analyzed by SDS-PAGE (lower) for PTP1B in the absence (upper panel) and presence (lower panel) of MSI-1436. Lanes 1-9 are fractions eluted from the column and lane M contains molecular weight markers. (Full blot image **Supplementary Fig. 21**).

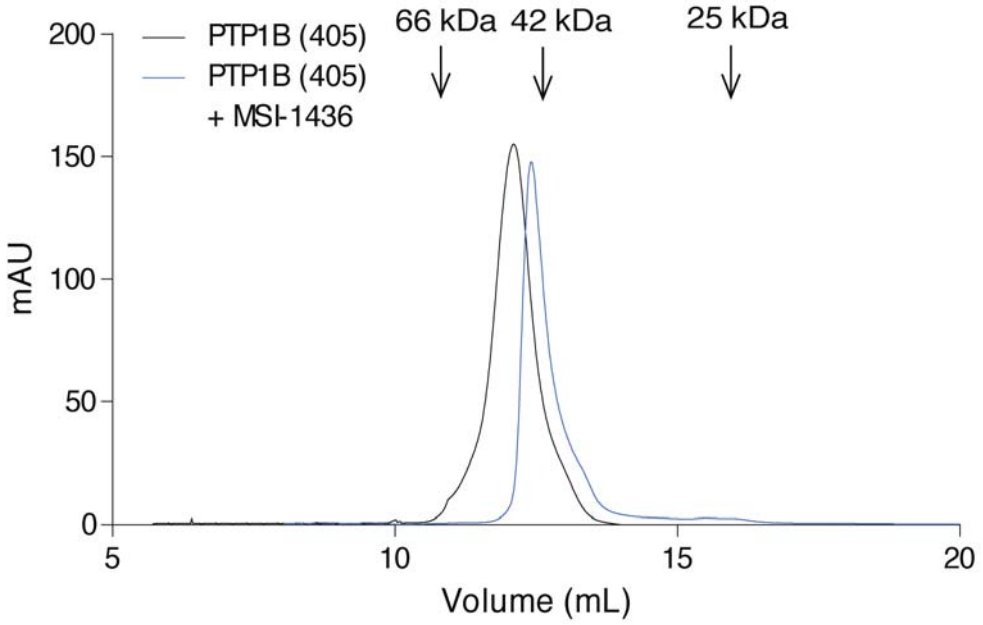

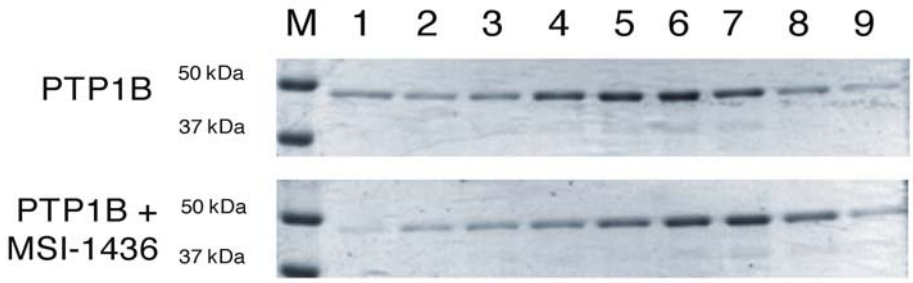

Supplementary Figure 5. Gel filtration analysis of $PTP1B_{1-321}$ in the absence and presence of MSI-1436

Elution profile of $PTP1B_{1-321}$ in the absence (black) and presence (blue) of MSI-1436. In both cases $PTP1B_{1-321}$ eluted as a monomer. The elution volumes were used to calculate the molecular weight of 37k in both the absence and presence of MSI-1436. The elution of molecular weight standards is indicated by arrows.

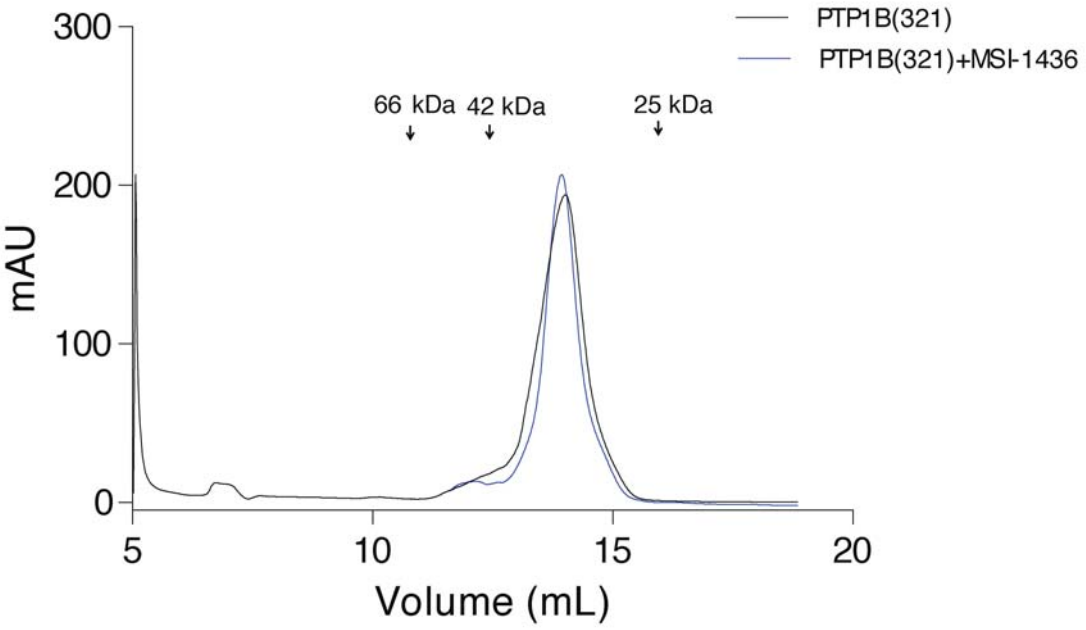

Supplementary Figure 6. Effect of MSI-1436 on limited proteolysis of $PTP1B_{1-405}$ with trypsin.

a and b. These data represent replicates of the experiment presented in **Figure 2a**, to illustrate the reproducibility of the analysis. Two separate repeat experiments (panels A and B) are shown involving SDS-PAGE following limited proteolysis of $PTP1B_{1-405}$ with trypsin in the absence (left) and presence (right) of MSI-1436. The procedure was as described in **Figure 2a**. Reactions were terminated with SDS sample buffer, and the digested products were analyzed by 20% SDS-PAGE and stained by Coomassie blue.

c. SDS-PAGE following limited proteolysis of $PTP1B_{1-405}$-L192A/S372P with trypsin in the absence (left) and presence (right) of MSI-1436. Purified $PTP1B_{1-405}$-L192A/S372P (2 μM) was incubated without (left) or with (right) 5 μM of MSI-1436 at a molar ratio of 1:10, 0.5:10, 0.25:10, 0.125:10, 0.06:10,0.03:10, 0.01:10, 0.005:10, 0:10 from left to right respectively. Reactions were terminated with SDS sample buffer, and the digested products were analyzed by 20% SDS-PAGE and stained by Coomassie blue.

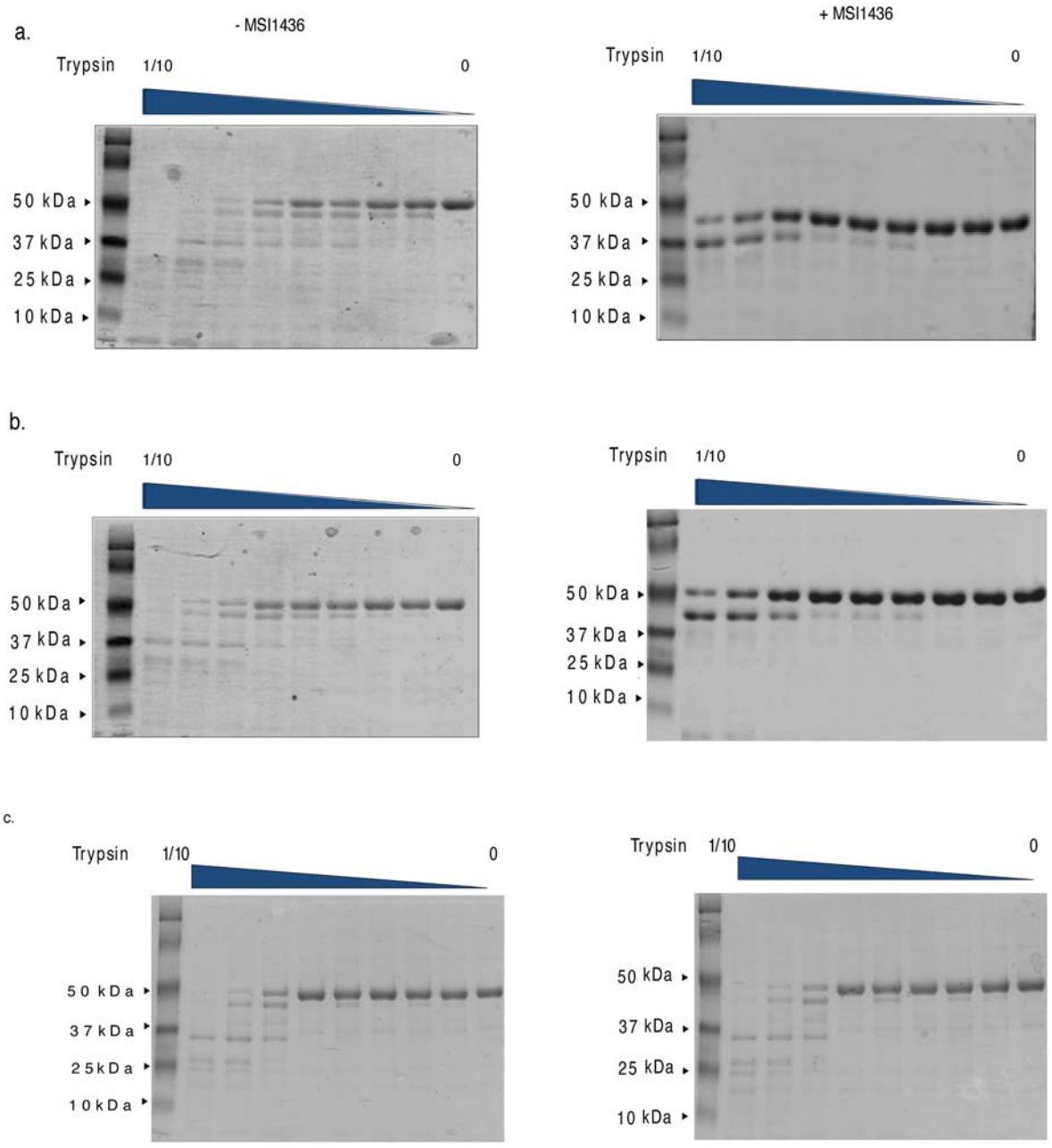
a.
- MSI1436
Trypsin
1/10
0
50 kDa
37 kDa
25 kDa
10 kDa
+ MSI1436
Trypsin
1/10
0
50 kDa
37 kDa
25 kDa
10 kDa
b.
Trypsin
1/10
0
50 kDa
37 kDa
25 kDa
10 kDa
Trypsin
1/10
0
50 kDa
37 kDa
25 kDa
10 kDa
c.
Trypsin
1/10
0
50 kDa
37 kDa
25kDa
10kDa
Trypsin
1/10
0
50 kDa
37 kDa
25 kDa
10 kDa

Supplementary Figure 7. Effect of MSI-1436 on CFP-PTP1B$_{1-321}$-YFP

Representative spectra from the experiment in which CFP-PTP1B$_{1-321}$-YFP was titrated with the inhibitor MSI-1436, covering a concentration range of 0 – 5 μM in which no FRET was observed in the absence or presence of the inhibitor.

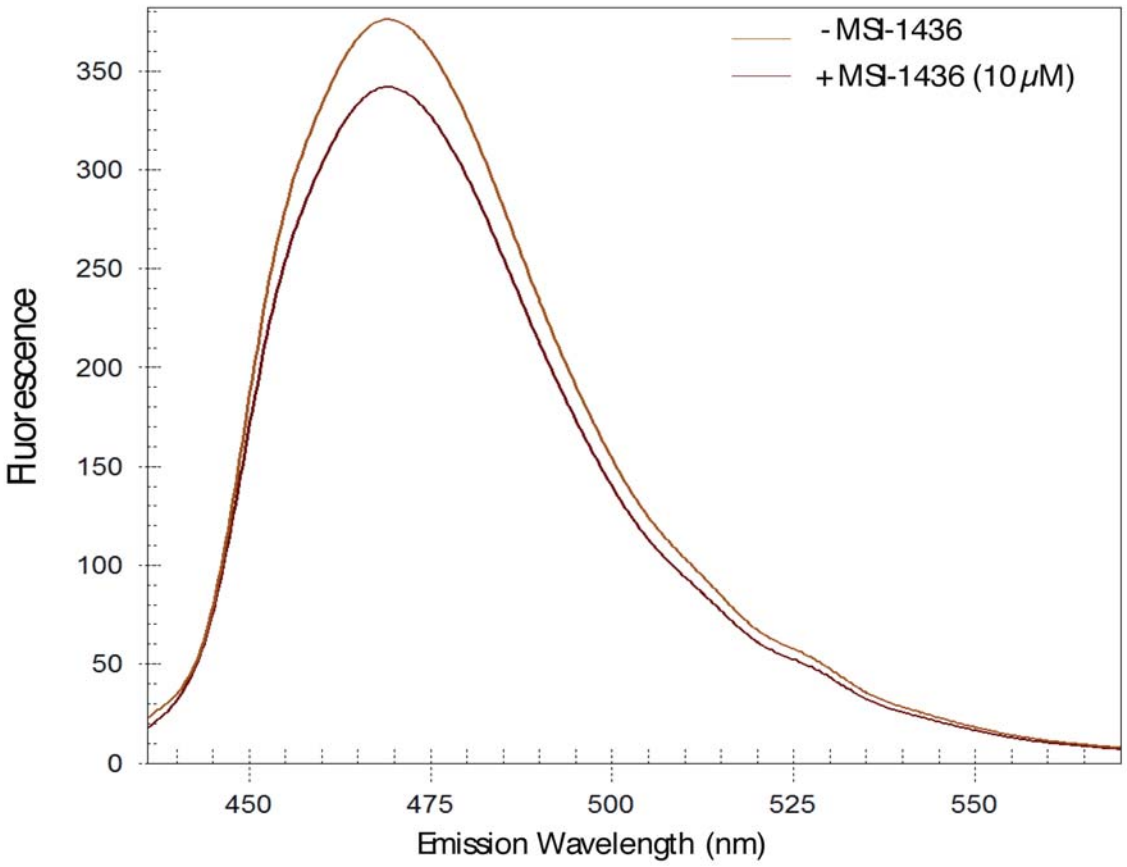

Supplementary Figure 8. PTP1B residues 300-393 were flexible and predominantly disordered.

Overlay of the 2D [^{1}H,^{15}N] TROSY spectra of PTP1B$_{1-301}$ (black) and PTP1B$_{1-393}$ (purple), as in **Fig. 3a,** but in reverse order.

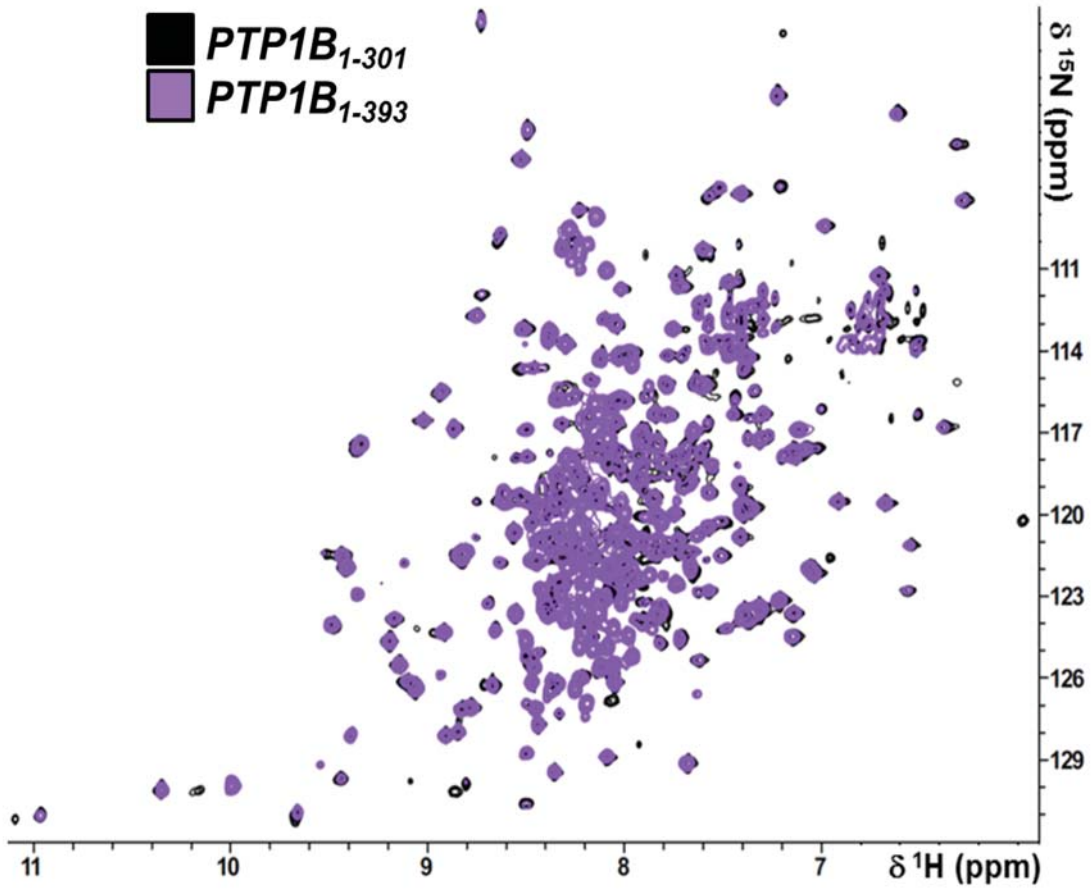

Supplementary Figure 9. PTP1B residues were perturbed upon MSI-1436 binding

a-d. Comparison of experimental (blue) and back-calculated (red) secondary chemical shifts for **(A)** $^{13}C\alpha$, **(B)** $^{13}C\beta$, **(C)** $^{1}H_N$, and **(D)** ^{15}N nuclei from a selected ASTEROIDS ensemble comprising 100 conformers.

e. Local conformational sampling derived from experimental chemical shifts (blue, green, red and magenta). Populations in four regions of Ramachandran space are shown compared to the statistical coil sampling (black). The populations are averaged over five independent ASTEROIDS selections of 100 structures. The Ramachandran space was divided into four regions defined as follows: αL {$\varphi > 0°$}; αR {$\varphi < 0$, $-120° < \psi < 50°$}; βP {$-100° < \varphi < 0°$, $\psi > 50°$ or $\psi < -120°$}; βS {$-180° < \varphi < -100°$, $\psi > 50°$ or $\psi < -120°$}. The populations of these quadrants are denoted p(αL), p(αR), p(βP) and p(βS), respectively.

f. Comparison of the distribution of the radius of gyration of the Flexible-Meccano pool (blue) and that of ten selected ASTEROIDS ensembles each comprising 100 conformers (red).

g. Contact maps showing chain proximity in the ensembles selected using ASTEROIDS on the basis of the experimental data. Plots are averaged over ten equivalent ensemble selections. *Left:* Logarithmic representation of the average distance between all $^{\alpha}C$ atoms in the protein. Distances between atoms in the folded domain simply represent the distances in the crystal structure. *Right:* Logarithmic plot of the ratio between the average distance (equation 1) in the ensembles selected using ASTEROIDS and the pool of conformers. Only the disordered region is shown, highlighting compaction of the chain via contacts between regions 330-360, and a positioning of this same region on average farther from the folded domain than is allowed on the basis of simple steric hindrance.

Average distances between sites were calculated as:

$$\Delta_{ij} = \log\left(\left\langle d_{ij}\right\rangle \middle/ \left\langle d_{ij}^{0}\right\rangle\right) \qquad \text{(Equation 1)}$$

d_{ij} is the distance in any given structure of the ASTEROIDS ensemble between sites i and j, and d^0_{ij} is the distance in any given structure of the reference ensemble (with no specific selection) between sites i and j.

h. Comparison of experimental (red) and back-calculated (blue) small angle X-ray scattering curve from a selected ASTEROIDS ensemble comprising 100 conformers.

Supplementary Figure 9

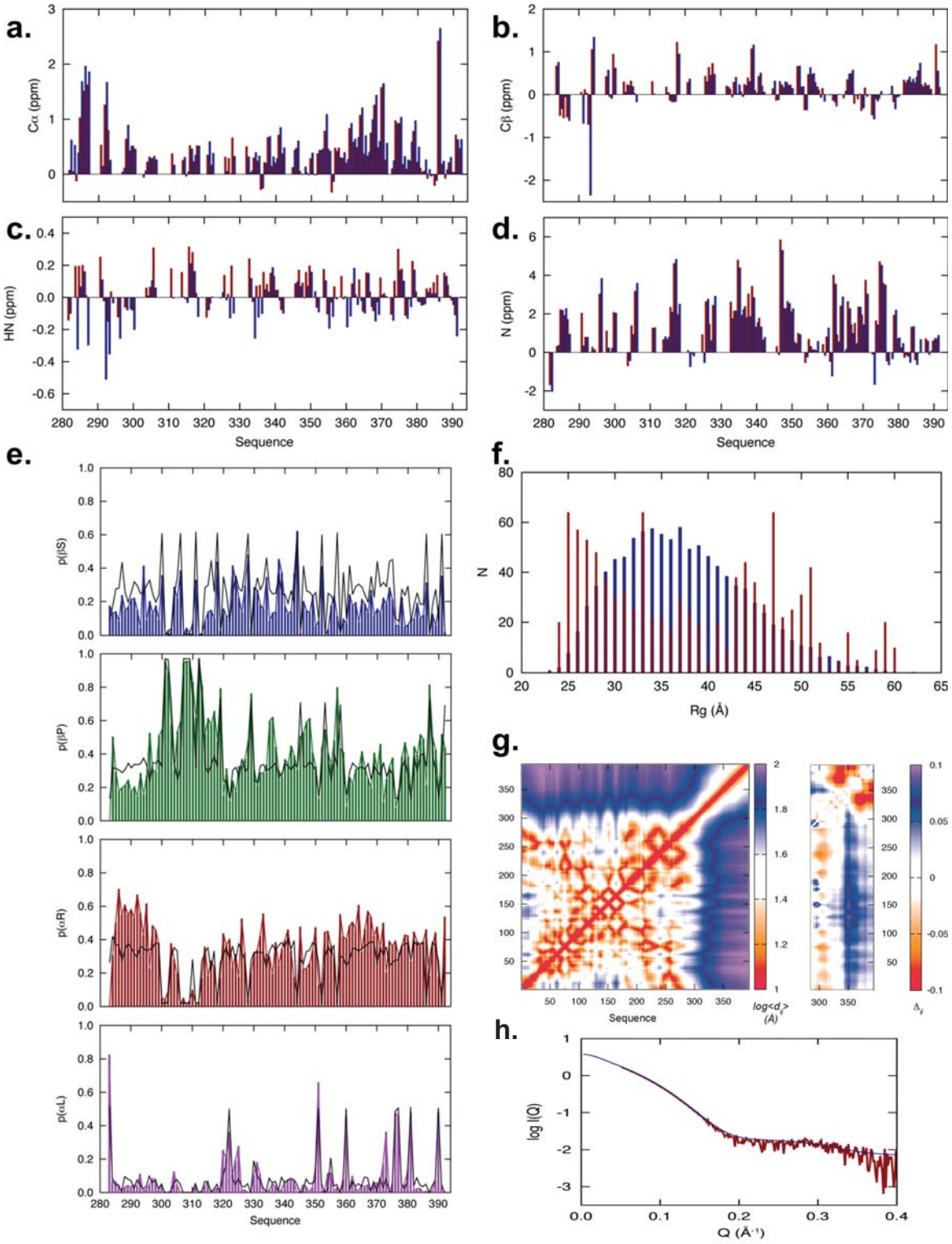

Supplementary Figure 10. Effect of mutations in the C-terminus of PTP1B on inhibition by MSI-1436

Sequential deletions from the C-terminus of $PTP1B_{1-405}$ (left). Bar graph to show the percent inhibition of the truncated forms of PTP1B at varying concentrations of MSI-1436 (0-10 μM) (right). Data represent mean ± s.e.m from three independent experiments.

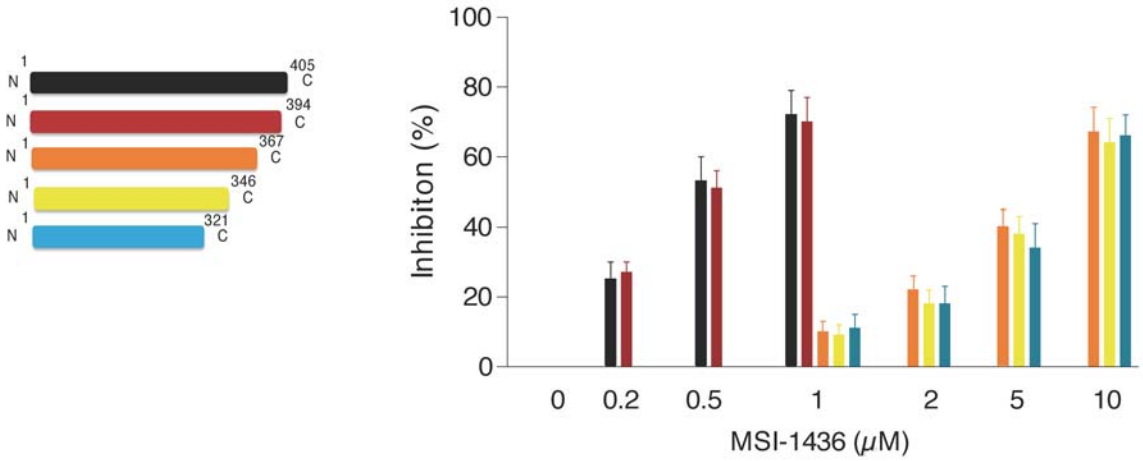

Supplementary Figure 11. Identification of the second binding site for MSI-1436 in PTP1B

a. Model showing the previously characterized allosteric site in PTP1B (exosite) where residues critical for the inhibitor binding in alpha 6 and alpha 7 helices are highlighted (upper panel). Mutational analysis of the exosite (lower panel). Each PTP1B mutant was assayed with increasing concentrations of MSI-1436 (0–10 μM) using 10 uM DiFMUP as substrate. The phosphatase activity in the presence of MSI-1436 is represented as percent activity relative to the total phosphatase activity observed in the absence of the inhibitor for WT $PTP1B_{1-405}$ (●), L192A (■), E276A (♦), M282A (▼), F196A (▲). Data represent mean ± s.e.m from three independent experiments.

b. Isothermal titration calorimetry analysis**.** A binding thermogram measured for $PTP1B_{1-405}$-L192A/S372P is shown. Non-linear least square curves (lower panel) could not be used to calculate the Kd indicating the lack of MSI-1436 binding to the mutant.

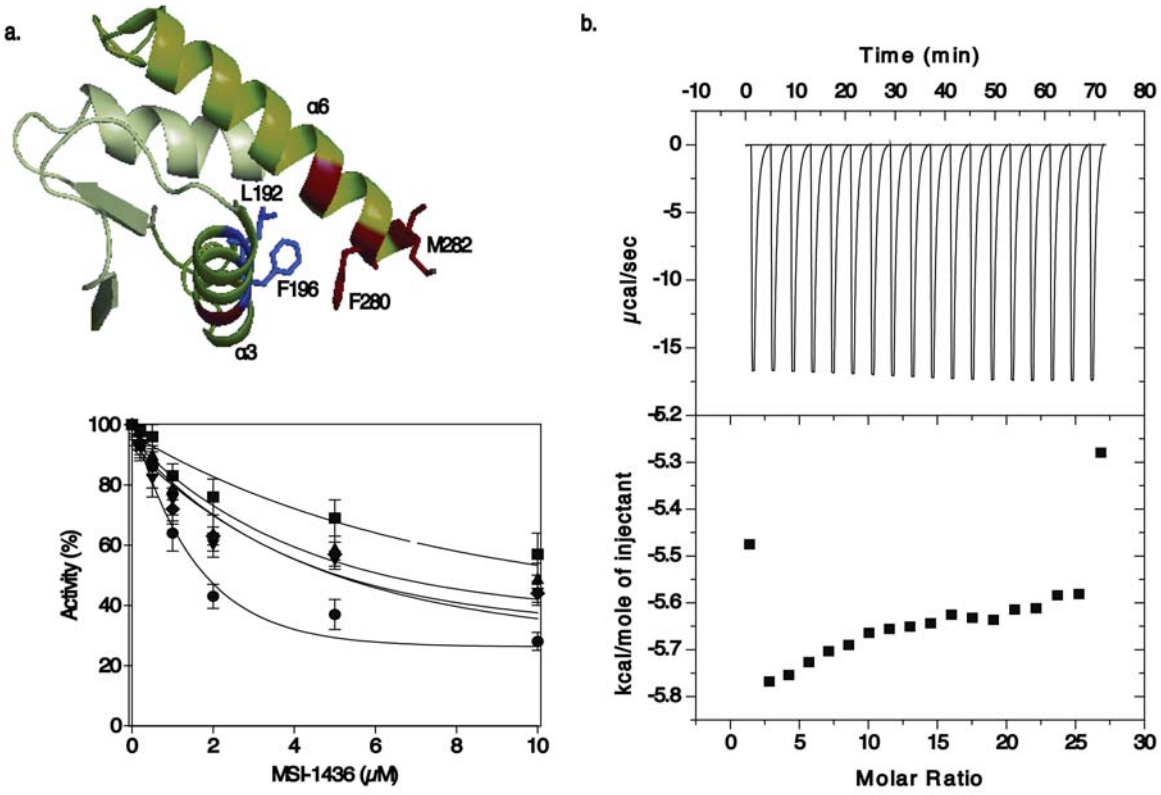

Supplementary Figure 12. Effect of the allosteric inhibitor of PTP1B, MSI-1436, in cell and animal models of HER2-positive breast cancer

a. 3-D Morphogenesis assays. MCF10A-AN mammary epithelial cells were grown in 3D culture in the absence (upper panels) or presence (lower panels) of AP1510 (1μM, to activate HER2), in the absence (left panels) or presence (right panels) of 5 μM MSI-1436. Data are representative of three independent experiments that were performed in duplicate.

b. Increased migration of MCF10A-AN mammary epithelial cells in the presence (filled bars) compared to the absence (open bars) of AP1510 (1μM, to activate HER2). Migration was attenuated by inhibition of PTP1B, either by expression of PTP1B shRNA or treatment with MSI-1436. Data are representative of three independent experiments that were performed in duplicate.

c. Migration of HER2 positive (MCF10A-AN, BT-474, SKBR3) and negative (MCF-7 and MDA-MB-231) cells was quantitated in Boyden chambers without (white bars) or with (black bars) MSI-1436 (5 μM), as indicated.

d. Cell proliferation of a panel of breast cancer cells was monitored in the absence and presence of MSI-1436 using the Cell-titer Glow assay. Data represent mean ± s.e.m from three independent experiments. At least 8 random fields were counted and the data from all fields were used to determine the average number of migrating cells per field. The experiment was repeated three times and error bars represent S.E.M.

e. Annexin/Propidium iodide staining of a panel of breast cancer cells was monitored in the absence and presence of MSI-1436. Data are presented as % apoptotic cells relative to controls in the absence of MSI-1436. Data represent mean ± s.e.m from three independent experiments.

Supplementary Figure 12

a.

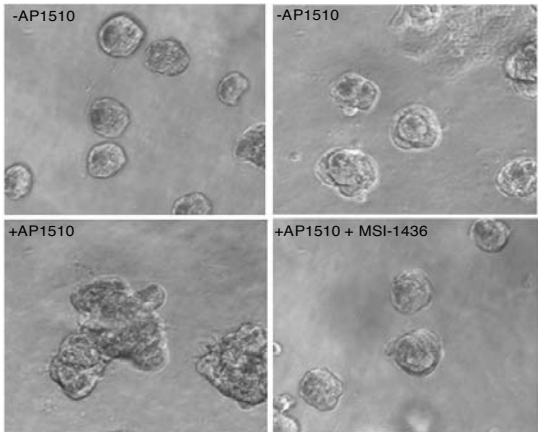

b.

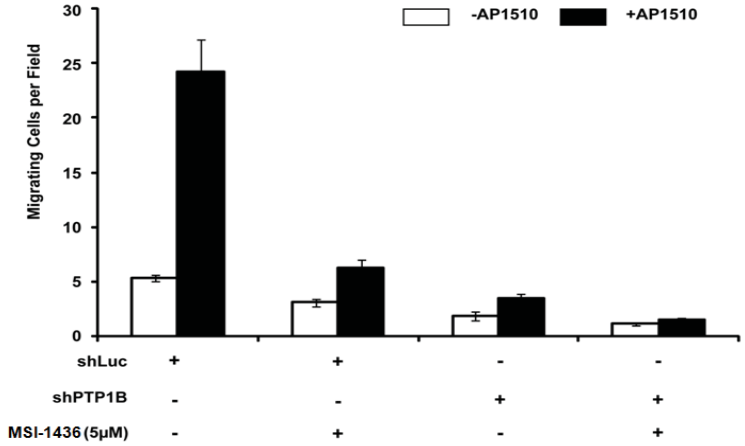

c.

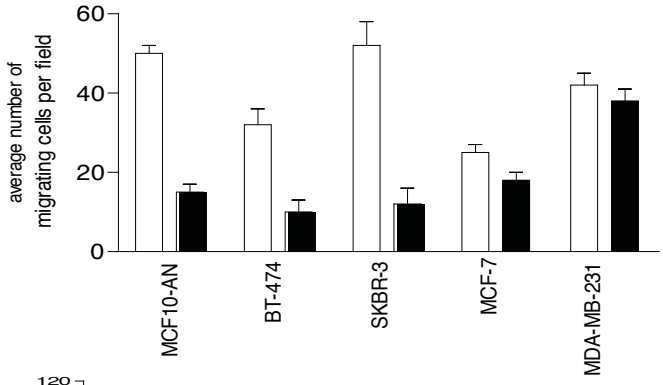

d.

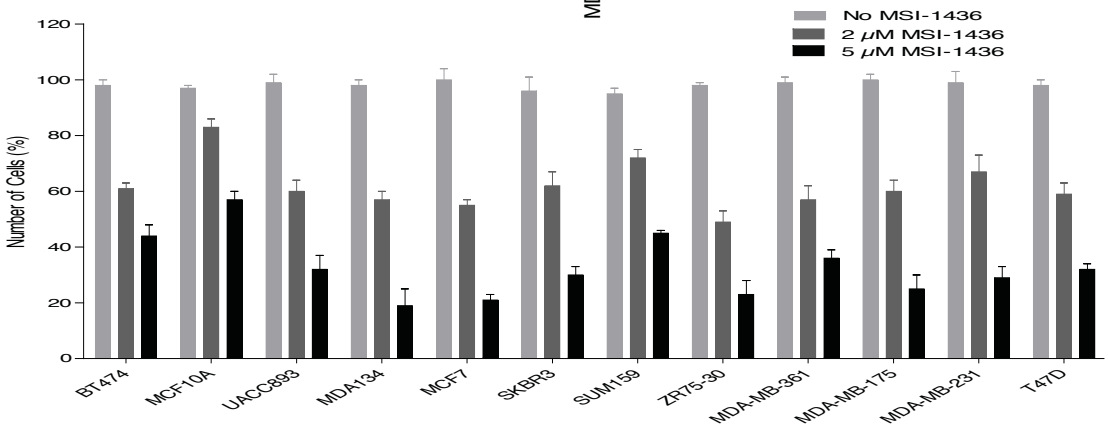

e.

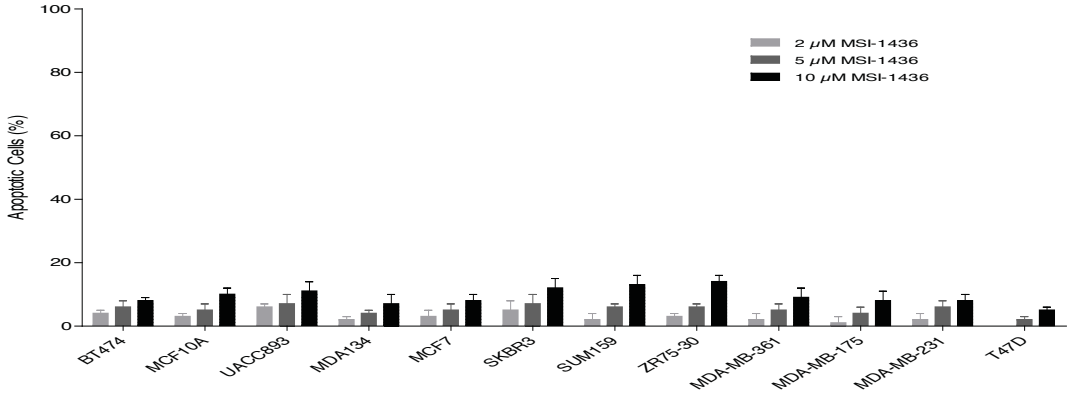

Supplementary Figure 13. Effects of MSI-1436 on signaling in breast tumors from NDL2 mice

a. Breast tumor tissue lysates obtained from control and MSI-1436-treated animals (from 4 different tumors from NDL2 animals represented as 1, 2, 3 and 4) were analyzed by immunoprecipitating pTyr proteins with antibody (4G10) and immunoblotting with antibody to p62DOK (upper panel). To ensure equal loading, lysates were directly loaded and probed using anti-p62 DOK (lower panel).

b. The samples were analyzed for phosphorylation of p42/p44 MAPK with a phosphospecific antibody, and the blot was stripped and re-probed for p42/44 MAPK protein.

(Full blot image **Supplementary Fig. 22**).

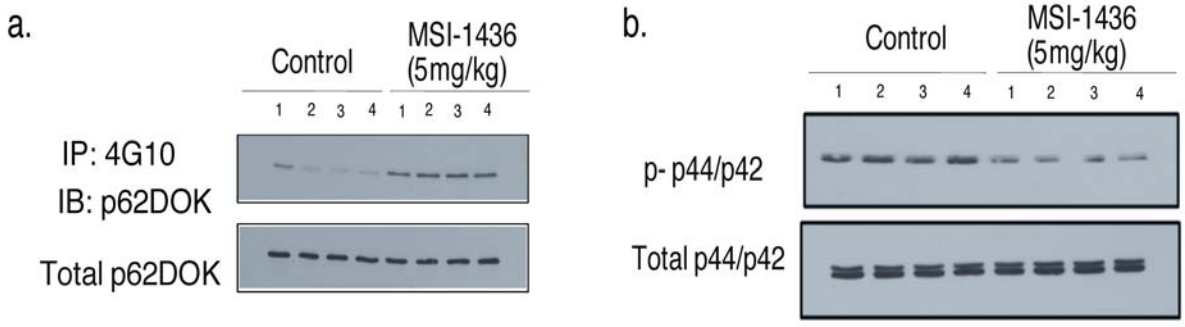

Supplementary Figure 14. Mechanism for coupling of MSI-1436 to NHS-activated Sepharose beads

MSI-1436 was immobilized on magnetic beads through covalent linkage using its primary amine group.

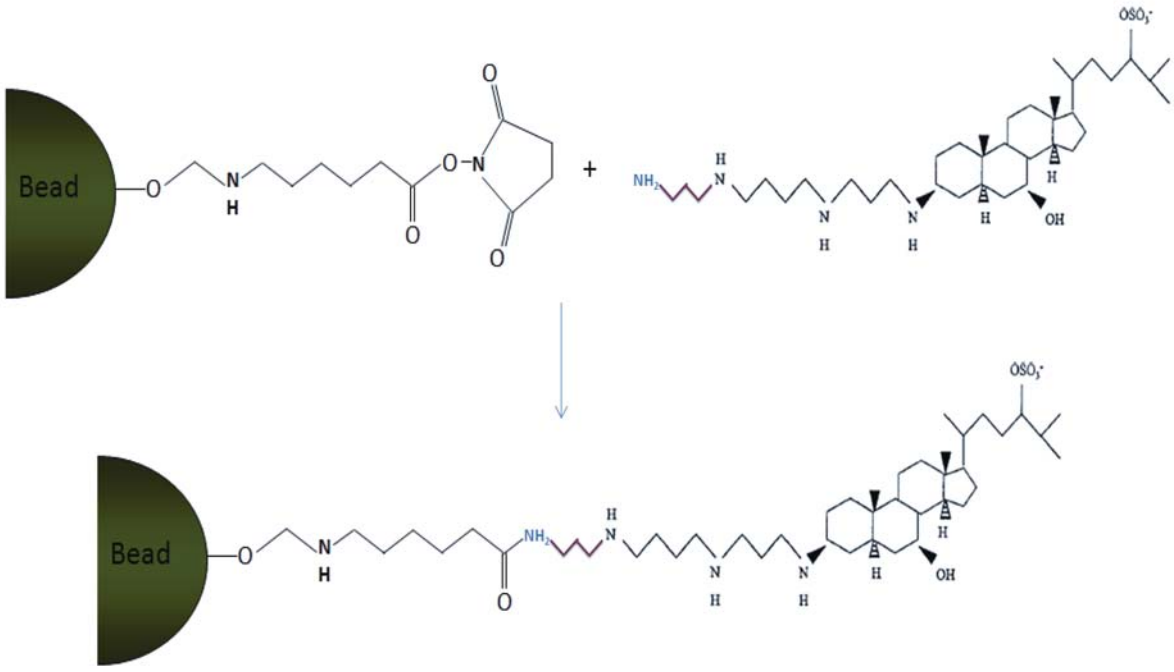

Supplementary Figure 15. MSI-1459 (3β-spermine, 5α, cholenic acid methyl ester), a structurally related analog of MSI-1436, was inactive as an inhibitor of PTP1B

The phosphatase activity of PTP1B was monitored using DiFMUP (10 uM) as substrate in the presence of varying concentrations of MSI-1459 (0-10 μM, closed square) or MSI-1436 (0-10 μM, closed circles), respectively. Data represent mean ± s.e.m of three independent experiments.

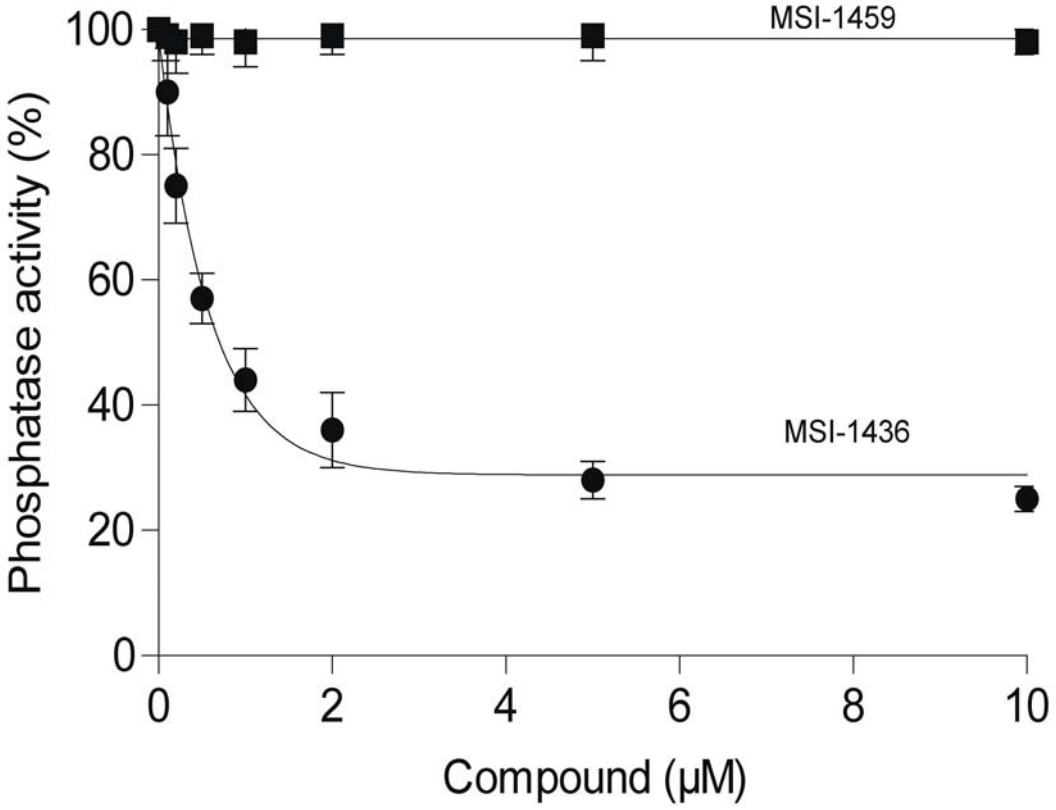

Supplementary Figure 16. Affinity chromatography on MSI-1436-conjugated beads

a. MSI-1436 immobilized to NHS-activated Sepharose beads was incubated with recombinant $PTP1B_{1-321}$ or $PTP1B_{1-405}$ in vitro. MSI-1459 coupled to beads was used as a negative control.

b. MCF-10A cell lysate was incubated with MSI-1436 bound beads for 30 minutes at 4 ˚C. The beads were washed and the samples were subjected to SDS-PAGE and silver staining (left) or immunoblotting with anti-PTP1B (FG6) antibody (right).

c. Tumor lysate was incubated with MSI-1436 immobilized to NHS-activated Sepharose beads for 30 minutes at 4 ˚C. The beads were washed and the samples were subjected to SDS-PAGE and silver staining (upper panel). Both beads and supernatant were subjected to immunoblotting using anti-PTP1B (FG6) antibody (lower panel) to demonstrate that PTP1B was cleared from the lysate by immobilized MSI-1436.

a.

Recombinant PTP1B

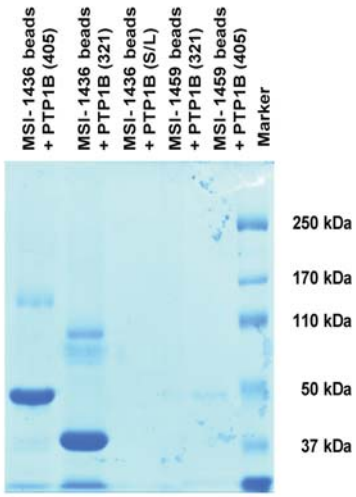

b. Cell lysate (MCF10A)

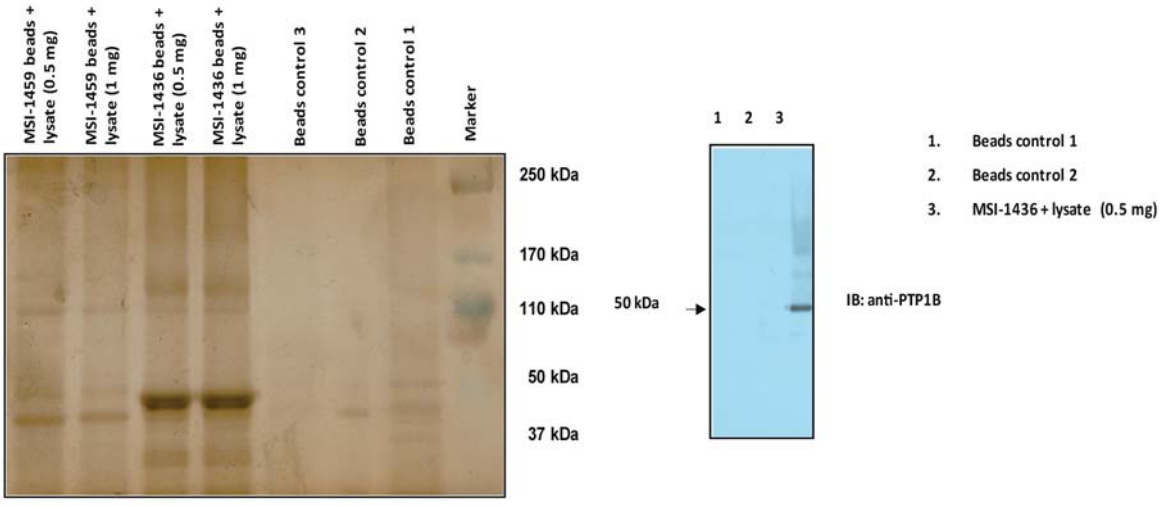

Supplementary Figure 17. A tumor xenograft study to demonstrate that PTP1B was a major target of MSI-1436 *in vivo*.

The effects of PTP1B depletion and re-expression on sensitivity of BT474 cell-derived tumors to MSI-1436 (5 mg/kg) were examined. Following suppression of PTP1B with specific shRNA, the cells were infected with retrovirus encoding WT-PTP1B and L192A/S372P-PTP1B and subsequently positive clones were selected. Each mouse used in the study received 5 X 10^6 cells as indicated and the study was conducted with 6 mice in each group. The data illustrate the time course of tumor development.

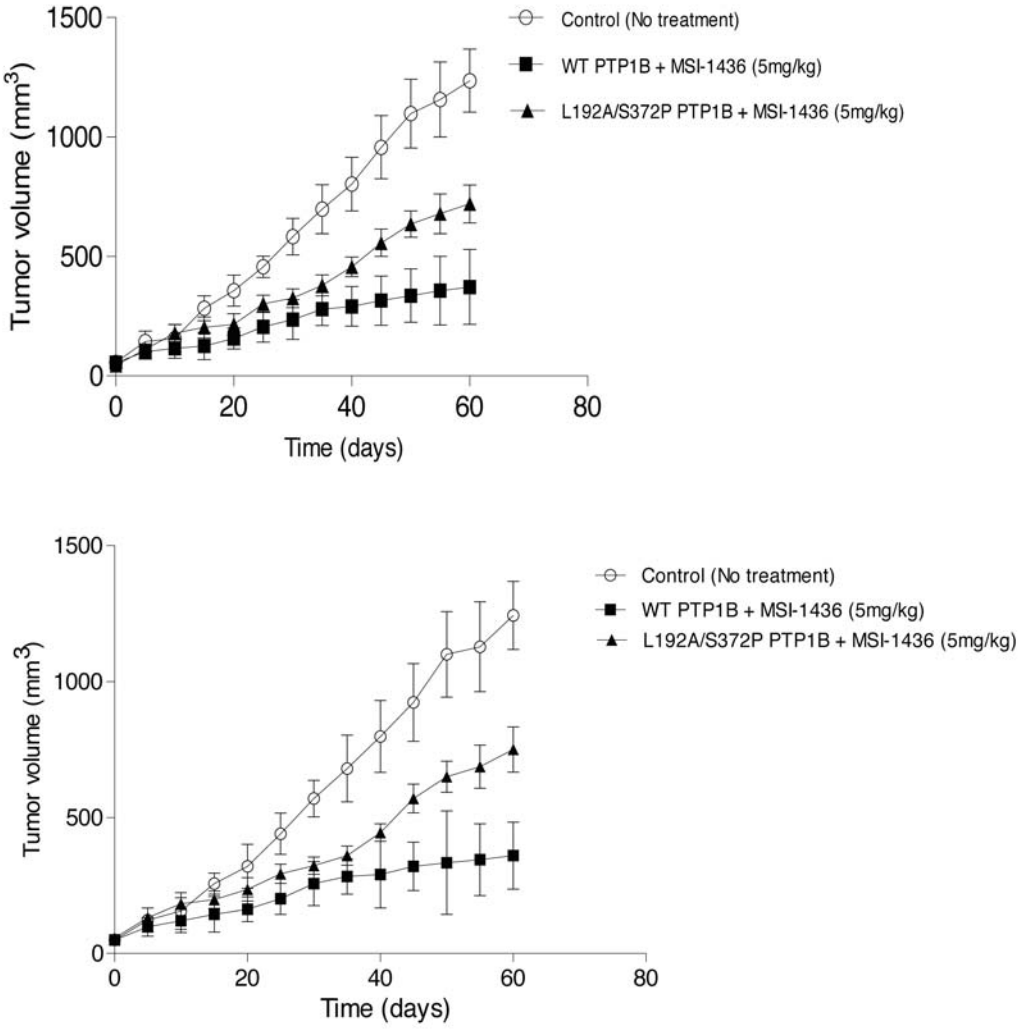

Supplementary Figure 18. Sequence similarity between PTP1B and a cholesterol-binding site in the β-andrenergic receptor

A cholesterol binding site in the β-andrenergic receptor is shown (left), which is adopted from the published crystal structure of β-andrenergic receptor complexed with cholesterol. (Right panel) The site in the C-terminus of PTP1B implicated in MSI-1436 binding displayed high sequence and potential structural similarity, suggesting a mechanism for MSI-1436 binding.

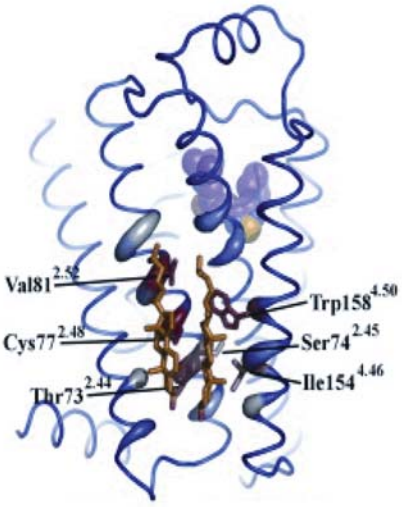

Adopted from Hanson M et al, Structure 16, 897-905 (2008)

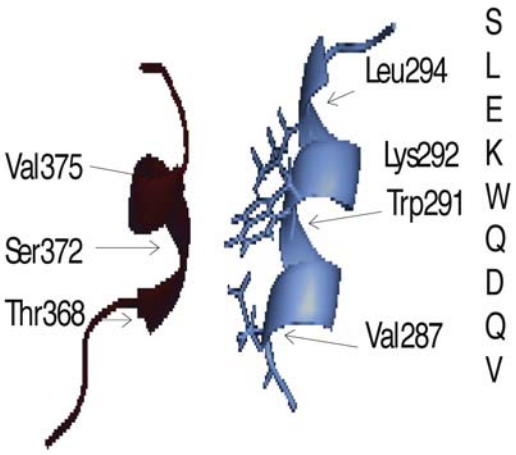

Supplementary Figure 19. Structure model for PTP1B (1-405) with two molecules of MSI-1436 docked to the two putative binding sites.

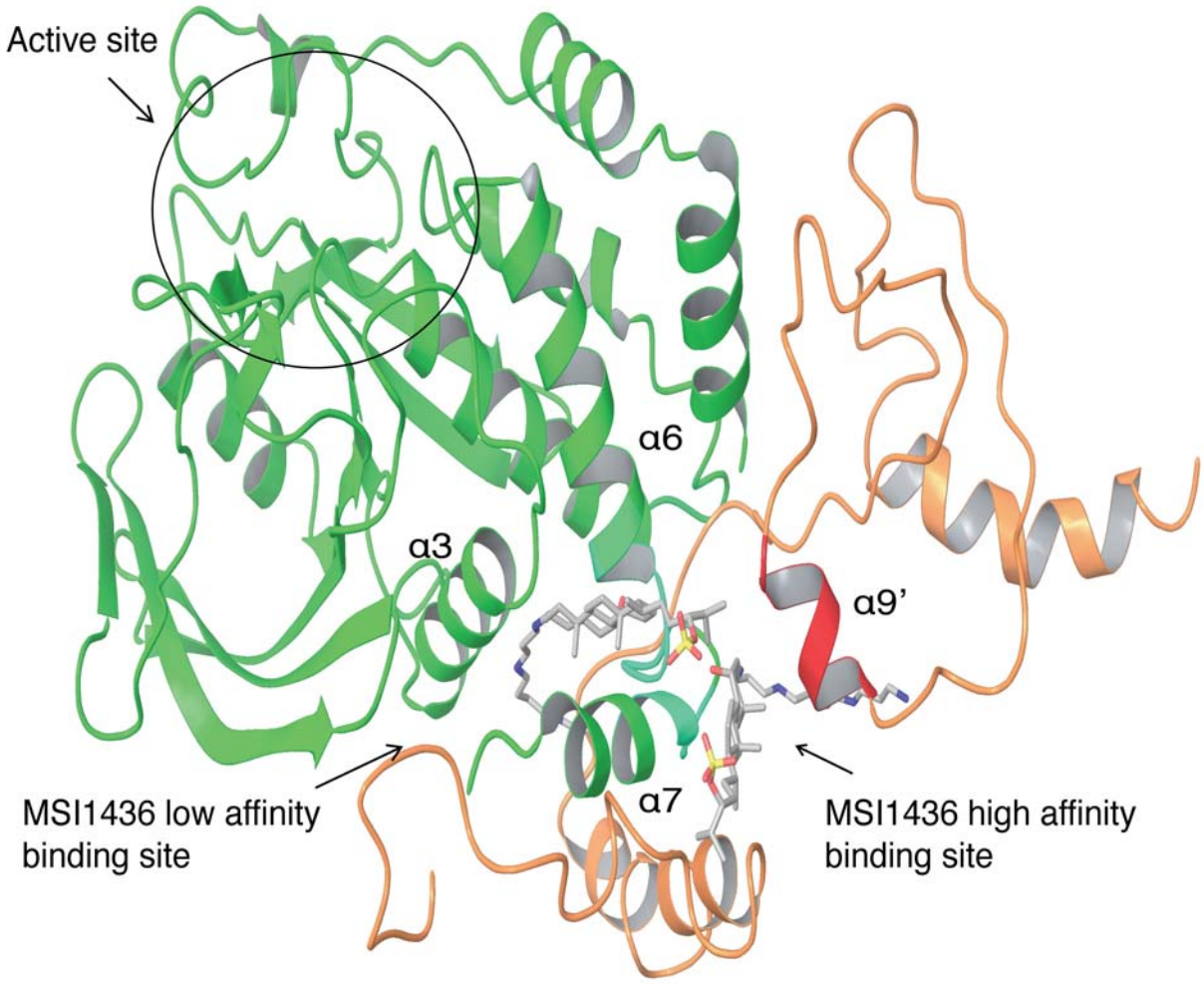

Supplementary Figure 20

Figure 6f (Full blot images)

Upper panel

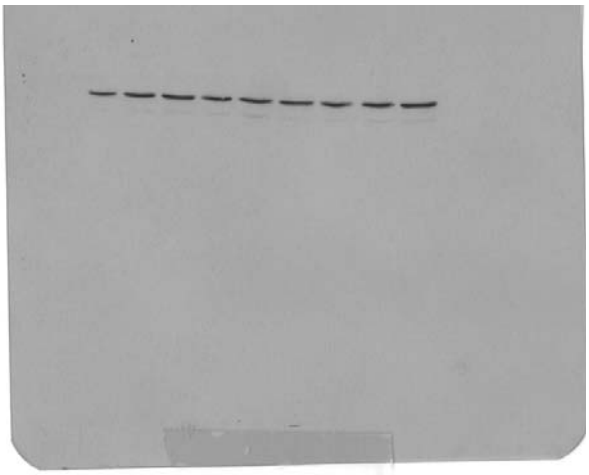

Lower panel

Supplementary Figure 21

Supplementary Figure 4 (Full gel images)

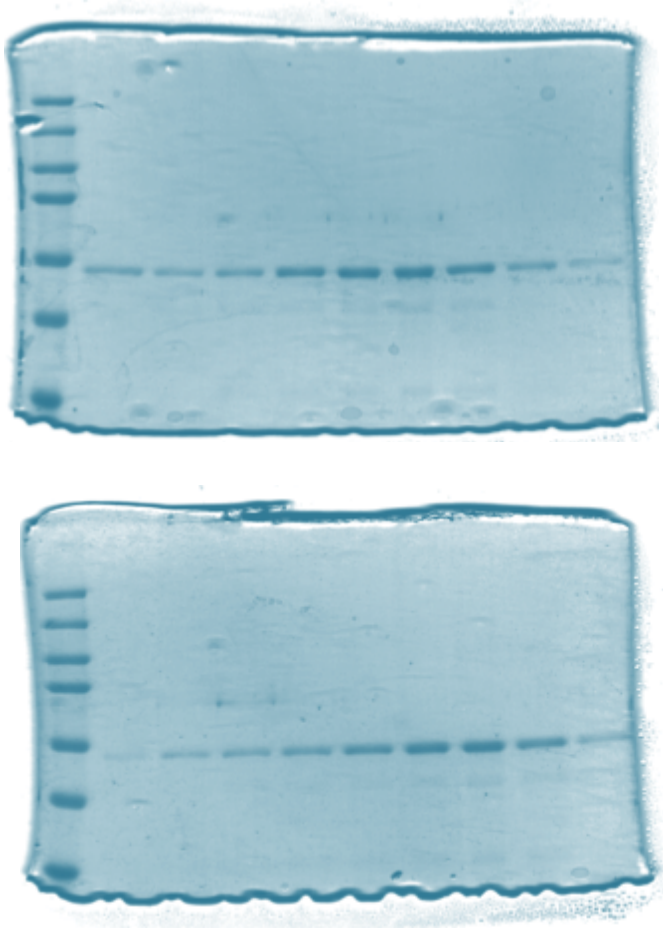

PTP1B - MSI-1436

PTP1B + MSI-1436

Supplementary Figure 22

Supplementary Figure 13 (Full blot images)

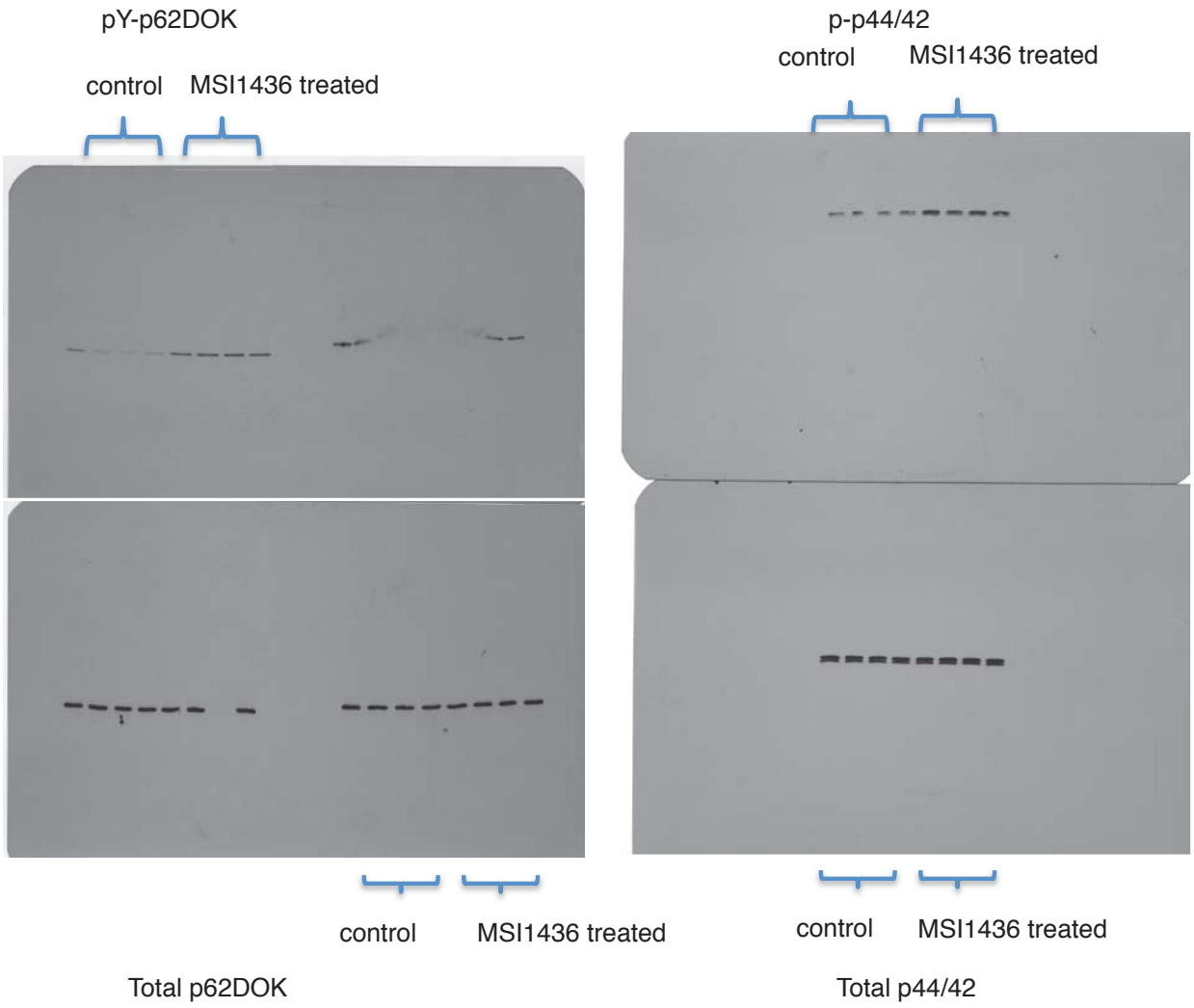

Supplementary Table 1. Specificity of MSI-1436 against a panel of PTPs

PTPs	K_m **(μM)**	K_{cat} **(s-1)**	K_i **(μM)**
PTP1B (1-405)	10	20	0.6
PTP1B (1-321)	8	40	4.0
TCPTP	25	18	6.0
PTP-PEST	57	13	40.0
LAR	42	20	20.0
CD-45	145	40	18.0
PTP-RR	90	13	25.0
PTP-alpha	83	6	-
PTP-mu	79	7	-
JSP1	120	9	-
PTEN	150	5	-

Supplementary Table 2- Effect of mutations in the exosite in $PTP1B_{1-405}$ and $PTP1B_{1-321}$ on inhibition by MSI-1436

Enzyme	K_i (μM)
PTP1B (1-405)	0.8
L192A PTP1B (1-405)	8.0
M282A PTP1B (1-405)	5.0
F196A PTP1B (1-405)	4.0
E276Q PTP1B (1-405)	4.5
F280A PTP1B (1-405)	6.0
PTP1B (1-321)	4.0
L192A PTP1B (1-321)	No inhibition
M282A PTP1B (1-321)	No inhibition
N193L PTP1B (1-321)	No inhibition
F280A PTP1B (1-321)	No inhibition

Supplementary Table 3 - Mutational analysis to define residues important for MSI-1436 binding to PTP1B

PTP1B (1-405)	K_{cat} (s^{-1})	K_i (μM)
Wild-type	30	0.8
Glu369Ala	27	1.2
Thr368Ala	30	1.5
Glu362Ala	32	1.0
Asn355Ala	29	1.8
Glu200Ala	25	2.7
Val287Met	22	12.0
Val287Ala	28	15.0
Lys292Ala	24	5.0
Lys292Pro	13	14.0
Leu294Ala	21	8.0
Ser295Phe	25	1.5

Supplementary Table 4 – Molecular Dynamics Simulation

Time (ps)	Total E (kJ/mol)	0.5 ps T (deg K)	Ave H (kJ/mol)	Ave T (deg K)	Ave H (300) (kJ/mol)
5.001	9915.2	300.6	-298.2	300.3	-308.3
10.000	9911.3	299.9	-351.3	300.1	-353.2
15.000	9907.5	300.4	-370.4	300.0	-370.2
20.001	9903.7	300.3	-374.8	299.9	-372.0
25.000	9985.1	300.5	-374.0	299.9	-370.7
30.000	10103.6	299.5	-394.7	299.9	-390.5
35.001	9609.7	299.4	-411.7	299.9	-407.2
40.000	9885.2	299.7	-423.1	299.9	-418.1
45.000	9835.3	300.1	-433.3	299.9	-428.2
50.001	9784.2	300.1	-431.7	299.9	-427.0

SUPPLEMENTARY NOTE

Homology Modeling

A homology model of the C-terminal segment of PTP1B was constructed using Schrodinger's Prime module. A BLAST sequence homology search encompassing residues [261-414] was first performed, affording 52 hits with 22-100 percent sequence homology in the NCBI PDB (non-redundant). Of these, 5 structures were selected for model building based on the following criteria: BLAST bit score, percent identities, percent positives, percent gaps, and X-Ray structure resolution. As hits with 100% identity corresponded to PTP1B database sequence entries, they were excluded, with the exception of 1EEN_A for which the structure of residues 261-282 was determined (helix 7). The following structures were then employed as templates for homology model building: 1EEN_A (1.9 Å); 2GRX_C (3.3 Å); 2KGL_A (NMR) ; 1RSS_A (1.9 Å); 3FEO_A (2.5 Å).

Once the alignments were performed, the comparative model building involved the following steps; firstly query backbone atoms were superimposed to the aligned template to identify identical side chain atoms. Then, insertions and deletions from the alignment were constructed and removed, respectively. *Ab initio* methods were used to close gaps using a backbone dihedral library. Finally, when the ligation of template junction was complete, minimization of non-conserved residues and residues for which no correspondence was found was performed. The "Build Structure" step used the OPLS_2005 force field, and reference residue side-chain and dihedral libraries extracted from the PDB for structure prediction. A total of five models were successively generated. For the final model, the 2GRX (TonB, a cytoplasmic membrane protein) template was excluded in favor of 2KGL (MESD, an endoplasmic reticulum-associated chaperone), affording a more complete structure with the least number of discontinuities.

Docking

The homology model was then ligated to a known PTP1B structure, 1t4j.pdb (Ref-Nat Struct Mol Bio 2004, V 11, pp 730-737), that was crystallized at 2.7 Å with an inhibitor bound in the allosteric site, locking the open-form conformation of the enzyme. Helices α3, α6 and α7 appear to be involved in stabilization of the closed-form of PTP1B in the presence of substrate; allosteric inhibitors prevent this closure. The $R_{371}SR_{373}$-containing helix of the C-terminus was implicated in allosteric inhibition. It may act as a hinge region and was rotated into proximity with helices α6 and α7. The now complete, predicted PTP1B structure was employed for docking studies with the allosteric inhibitor 1436.

Molecular Dynamics Simulation

PTP1B was prepared for minimization and dynamics simulations, as described for docking studies. A preliminary minimization of the PTP1B complex with two molecules of 1436 was performed using the steepest descents method with the OPLS 2005 force field and water as solvent over 3000 steps. Molecular dynamics calculations were then performed on the minimized structure. Molecular dynamics was done at 300K, 1.5 fs, 1 ps equilibration and 50 ps stimulation. The protein backbone was constrained, while the ligands and residues around the ligands were treated. A final minimization was performed using the Polak-Ribier conjugate gradient method over 500 iterations to a convergence of 0.05 Å RMSD. Final potential and kinetic energy were found to be -369.08 and 10305.46 kJ/mol respectively.

Polak-Ribier Conjugate Gradient Minimization:

Total Energy = -83173.5000 kJ/mol

Stretch = 7086.2427 kJ/mol

Bend = 4231.3643 kJ/mol

Torsion = 5448.0752 kJ/mol

Improper Torsion = 124.0153 kJ/mol

VDW = -2291.7546 kJ/mol

Electrostatic = -71704.9766 kJ/mol

Explicit Hydrogen Bonds = 0.0000 kJ/mol

Cross Terms = 0.0000 kJ/mol

Solvation = -26066.4688 kJ/mol

ASTEROIDS ensemble selections

Initially Cα, Cβ, N and H^N chemical shifts (CS) of PTP1B residues 282-393 (including helix α7) were analysed, to determine site-specific conformational sampling. Next, a pool of 10000 statistical coil conformers was generated using the program Flexible-Meccano[45,46], side chains were added using SCCOMP[47] and CS were calculated for each conformer using SPARTA[48]. ASTEROIDS[49] was used to select five sub-ensembles, each comprising 200 conformers on the basis of the experimental CS following an iterative procedure as previously described[50,51]. The errors used for the CS in the ASTEROIDS calculations were as follows: Cα and Cβ (0.1 ppm), N (0.2 ppm) and H^N (0.04 ppm).

Dihedral angles from the selected structures were extracted for each amino acid and used to build representative conformers of $PTP1B_{1-393}$. PTP1B residues 300-393 were connected to the catalytic domain PTP1B crystal structure (PDBid: 1SUG) by Flexible-Meccano using the amino acid specific conformational sampling derived by ASTEROIDS, creating a pool of 15000 conformers. This pool comprised 3 populations, which differ in the behaviour of helix α7: 1) In 5000 conformers α7 was maintained as identified in 1SUG and PTP1B residues 300-393 started C-terminal of α7; 2) in 7000 conformers residues 285-296 were assumed to be disordered and 3) in 3000 conformers, helix α7 was intact but no longer interacted with the surface of PTP1B. The rational for the selection from these different pools was 1) the initial

NMR CS analysis suggested only ~40% helical behaviour of α7 and 2) α7 has no corresponding electron density in numerous PTP1B crystal structures.

Side chains were added to all conformers using SCCOMP; CS and SAXS curves were calculated using SPARTA and CRYSOL[52], respectively. Ten sub-ensembles were selected using ASTEROIDS, comprising 100 conformers in each ensemble based on the experimental SAXS and CS data. Errors on the CS and SAXS data were adjusted to obtain an almost equal contribution from the two datasets in the selection procedure. The appropriate number of conformers in the selected ensembles was determined by obtaining the active χ^2 for independent ensemble selections comprising 25, 50, 75, 100, 125, 150, 175 and 200 conformers. A minimum was observed at 75-100 conformers. The agreement between experimental and back-calculated data was analysed for the best-fitting ensemble. Secondary CS were calculated using the random coil values of RefDB[16].

MSI-1436-PTP1B interaction in tumor xenografts

In order to examine the specificity of MSI-1436 in vivo, we followed the procedure above to compare its effects on the growth of orthotopic BT474 xenografts after RNAi-mediated suppression of PTP1B then rescue with either wild type or MSI-1436-resistant forms of PTP1B. We generated PTP1B-suppressed BT474 cells by infecting with retrovirus encoding PTP1B-specific shRNA. The infected cells were selected using puromycin and the knock-down efficiency (80-90%) was tested by immunobloting for PTP1B (FG6). PTP1B was then stably re-expressed in these cells. For this the *PTP1B* gene was cloned into a pwzl-vector with a different selection marker (hygromycin) so that positive clones could be successfully selected. To make the clone resistant to the shRNA used, we made 6-point mutations in the region of the gene targeted by the shRNA. We replaced the original sequence with degenerate codons so the amino acid sequence would not be altered. The cells were infected with retrovirus encoding

WT-PTP1B and L192A/S372P-PTP1B and subsequently positive clones were selected, which were propagated for several weeks to generate sufficient cells to perform the xenograft study. Each mouse used in the study received 5 X 10^6 cells and the study was conducted with 6 mice in each group.

It is important to note that there are significant technical challenges associated with such experiments. First, suppression of PTP1B by RNAi is not complete, so there remains a residual pool of wild type PTP1B, even in those cells that were “rescued” with MSI-1436-resistant PTP1B. Consequently, this residual pool of wild type PTP1B would remain sensitive to the effects of MSI-1436. Second, although the double point mutation in PTP1B (L192A-S372P) profoundly suppresses inhibition by MSI-1436, again a small residual level of inhibition remains. Therefore, when one considers the combination of low levels of residual wild type PTP1B and residual susceptibility of mutant PTP1B to inhibition by MSI-1436, coupled with the prolonged duration of the animal studies, one would anticipate that partial effects would be observed rather than a “black-and-white” response.